HHS Public Access

Author manuscript

Gynecol Oncol. Author manuscript; available in PMC 2022 February 01.

Published in final edited form as:

Gynecol Oncol. 2021 February ; 160(2): 427–437. doi:10.1016/j.ygyno.2020.11.009.

Development of a clinically relevant ovarian cancer model incorporating surgical cytoreduction to evaluate treatment of micro-metastatic disease

Christopher B. Morse[1,2], **Valentin Voillet**[3], **Breanna M. Bates**[2], **Edison Y. Chiu**[2], **Nicolas M. Garcia**[2], **Raphael Gottardo**[3], **Philip D. Greenberg**[2,4,*], **Kristin G. Anderson**[2,*]

[1]Division of Gynecologic Oncology, Department of Obstetrics and Gynecology, University of Washington, Seattle, WA 98195

[2]Program in Immunology, Clinical Research Division, Fred Hutchinson Cancer Research Center, Seattle, WA 98109

[3]Vaccine and Infectious Disease Division, Fred Hutchinson Cancer Research Center, Seattle, WA 98109

[4]Divison of Medical Oncology, Department of Medicine, and Department of Immunology, University of Washington, Seattle, WA 98195

Abstract

Objectives: Mouse models of ovarian cancer commonly transfer large numbers of tumor cells into the peritoneal cavity to establish experimental metastatic disease, which may not adequately model early metastatic spread from a primary tumor site. We hypothesized we could develop an ovarian cancer model that predictably represents micro-metastatic disease.

Methods: Murine ID8$_{VEGF}$ ovarian cancer cells were transduced to express enhanced luciferase (eLuc) to enable intravital detection of microscopic disease burden and injected beneath the ovarian bursa of C57Bl/6 mice. At 6 or 10 weeks after orthotopic injection, when mice had detectable metastases, hysterectomy and bilateral salpingo-oophorectomy was performed to remove all macroscopic disease, and survival monitored. Immunohistochemistry and gene expression profiling were performed on primary and metastatic tumors.

Corresponding authors: Kristin G. Anderson, PhD, Fred Hutchinson Cancer Research Center, Mail Stop D3-100, 1100 Fairview Ave N, Seattle, WA 98109-1024, ande8527@uw.edu; kganders@fredhutch.org, Philip D. Greenberg, MD, Fred Hutchinson Cancer Research Center, Mail Stop D3-100, P.O. Box 19024, 1100 Fairview Ave N, Seattle, WA 98109-1024, pgreen@uw.edu, Christopher B. Morse, MD, University of Washington Medical Center, Department of Obstetrics and Gynecology, Box 356460, Seattle, Washington 98195-6460, Phone: 206-543-3669 Fax: 206-543-3915, cbmorse@uw.edu.

*These authors contributed equally to the work.

Author contributions: Conceptualization, C.B.M., K.G.A. and P.D.G.; Methodology, C.B.M., K.G.A., V.V., R.G., and P.D.G.; Validation, V.V. and R.G.; Data Acquisition and Analysis, C.B.M., K.G.A., B.B., E.Y.C., and N.M.G.; Writing – Original Draft, Review and Editing, C.B.M., K.G.A., V.V., R.G., P.D.G.; Funding Acquisition, C.M.B., K.G.A. and P.D.G; Supervision, C.M.B., K.G.A., R.G. and P.D.G.

Results: eLuc-transduced ID8$_{VEGF}$ cells were brighter than cells transduced with standard luciferase, enabling *in vivo* visualization of microscopic intra-abdominal metastases developing after orthotopic injection. Primary surgical cytoreduction removed the primary tumor mass but left minimal residual disease in all mice. Metastatic sites that developed following orthotopic injection were similar to metastatic human ovarian cancer sites. Gene expression and immune infiltration were similar between primary and metastatic mouse tumors. Surgical cytoreduction prolonged survival compared to no surgery, with earlier cytoreduction more beneficial than delayed, despite micro-metastatic disease in both settings.

Conclusions: Mice with primary ovarian tumors established through orthotopic injection develop progressively fatal metastatic ovarian cancer, and benefit from surgical cytoreduction to remove bulky disease. This model enables the analysis of therapeutic regimens designed to target and potentially eradicate established minimal residual disease.

Introduction

Ovarian cancer is the most lethal of the gynecological cancers and the fifth leading cause of cancer deaths among women [1]. The current standard of care for advanced ovarian cancer involves cytoreductive surgery and chemotherapy, but despite advances in drug development and treatment approach, the mortality rate has changed little in the last 30 years [2]. Thus, the development and testing of novel therapies that can more effectively eliminate either large-volume or micro-metastatic disease are greatly needed. Potential options include new chemotherapy regimens, new targeted drugs, and also immunotherapies, as there is abundant evidence that ovarian cancer can be recognized by immune cells [3,4].

Preclinical mouse models of ovarian cancer commonly involve intraperitoneal injection of tumor cells to establish metastatic disease [5–7]. The syngeneic ID8 [5], ID8$_{VEGF}$ [6], or CRISPR edited ID8 mouse models [7] are often used for studies interrogating immune-related features of ovarian cancer because the tumor cells can be transferred into an immune-competent host animal and will develop immune-infiltrated suppressive tumor microenvironments (TME). Although the intraperitoneal ID8 or ID8$_{VEGF}$ mouse model simulates many histological and molecular features of advanced stage human ovarian cancer [8], little is known following the direct injection of large numbers of tumor cells into the peritoneum regarding the nature of the early events required for tumor engraftment and development, and if these events reflect the biology of human metastatic disease. Consequently, most studies initiate treatment regimens early after tumor cell inoculation in the peritoneal cavity [9,10], and results may reflect interference with tumor engraftment rather than targeting developing micro-metastatic and progressing metastatic disease. A model that establishes disease in a primary tumor location and allows for seeding of metastatic disease throughout the peritoneal cavity, disseminating from the primary tumor, may better simulate the natural events that occur in human metastatic disease. Moreover, metastatic tumors seeded from primary tumors that progress to histologically resemble advanced human disease should provide a more informative model for evaluating therapies targeting potentially undetectable micro-metastatic disease.

By the time disseminated disease has become established in animal models using intraperitoneal injection, surgical cytoreduction of the widespread disease is not feasible before initiating potentially curative therapies. As surgical cytoreduction is commonly employed and correlated with long-term survival in ovarian cancer patients [11,12], development of an immune-competent, surgically relevant model may be useful for designing and testing preclinical strategies for effective treatment of minimal residual disease. Models that simulate the establishment of micro-metastatic disease in an immune-competent host are unfortunately limited. We hypothesized that we could develop a model for micro-metastatic residual disease that establishes tumors that recapitulate human disease, and that could be used for intervention studies of residual, visibly undetectable, micro-metastatic disease, which, if left untreated, would ultimately be fatal. We now describe the development of a mouse model of ovarian cancer in which cytoreductive surgery can be used to provide therapeutic benefit by resecting the primary disease burden while preserving metastatic minimal residual disease.

Methods

Production of cell lines

The $ID8_{VEGF}$ cell line (Matthias Stephan) was thawed, washed, resuspended, and plated in growth media (1L DMEM plus 100 mL fetal bovine serum, 10 mL penicillin-streptomycin, and 1.1 mL insulin-transferrin-selenium (ITS)). Cells were expanded at 37°C with 5% CO_2 and passaged every 48–72 hours, or when 90% confluent. To optimize visualization of *in vivo* tumorigenesis, $ID8_{VEGF}$ cells were transduced with an enhanced luciferase (eLuc) construct containing GFP [13]. Following transduction, GFP^+ cells were sorted (BD Biosciences, FACSAria), expanded and rescreened to establish a pure GFP^+ $ID8_{VEGF\text{-}eLuc}$ cell line.

In vitro and in vivo IVIS imaging

$ID8_{VEGF\text{-}eLuc}$ cells were plated at varying concentrations in a 96-well black polystyrene microplate (Corning), with 200 μL of D-Luciferin (150g/mL) added to each well, incubated briefly, and then imaged with the IVIS Spectrum and Living Image Software 4.7.2 (Perkin Elmer). Ten minutes before *in vivo* imaging, mice were anesthetized with isoflurane, clipped, and D-Luciferin (15mg/mL) injected intraperitoneally (100L/g). Biodistribution of the tumor nodules was quantified in photons per second. Following orthotopic tumor injection, mice were serially imaged every 2–4 weeks to assess tumorigenesis.

Animal surgery - orthotopic injection

C57BL/6 mice were purchased from Jackson Labs and housed in the Comparative Medicine Animal Facility under regular housing guidelines. All animal experiments were IACUC approved and adhered to standard institutional protocols. All surgical procedures were performed under a stereomicroscope (Leica MZ6). At approximately 8 weeks of age, mice were anaesthetized with isoflurane, clipped, prepped, and sterily draped for surgery in a prone position. After confirming adequate anesthesia, a single dorsal incision was made to the right of the midline, the right ovary was exteriorized and stabilized with a bulldog clip, and 1×10^6 $ID8_{VEGF\text{-}eLuc}$ cells suspended in sterile PBS were injected directly under the

ovarian bursa using a 30g Hamilton syringe [14,15]. The techniques for orthotopic injections were initially optimized using injections of dilute trypan blue dye to confirm that the procedure resulted in no spillage upon insertion, injection or withdrawal of the syringe from the ovarian bursa. The ovary was then returned to the abdominal cavity, the cavity closed with a single interrupted suture of 4–0 Polysorb, and the skin closed with surgical clips. The mice were then monitored closely for 7–10 days, following institutional surgical protocols. Daily weights were obtained during the recovery period and weekly thereafter. 14–18 days after recovery from the orthotopic tumor cell injection, IVIS imaging was performed to assess potential spread from leakage from the tumor injection site, and all luminescent signal was confirmed to be confined to the injected ovary.

Animal surgery - surgical cytoreduction

At 6- or 10-weeks after orthotopic injection, after the presence of micro-metastatic disease was confirmed with IVIS imaging (described above), a second surgery was performed to replicate ovarian cancer cytoreductive surgery. The goal was to completely resect the primary tumor, removing bilateral ovaries, fallopian tubes, uterine horns, uterus, and any macroscopic disease, and ideally achieving no gross residual disease. Mice were anesthetized as described above and prepped for surgery in a supine position; a 1.5–2.0 cm ventral midline incision was made, the abdomen entered and a small self-retaining retractor placed for adequate visualization. The reproductive tract, including the ovaries, fallopian tubes, and uterus were externalized and the blood supply to the ovaries was cauterized bilaterally using a cautery pen (Gemini Cautery System). A single 4–0 Polysorb suture was placed at the base of the uterus, and the specimen removed. The abdomen was closed with a running 4–0 Polysorb suture and the skin closed with clips. Routine recovery and postoperative monitoring were performed. In all surgeries, there was no evidence of macroscopic disease outside of the ovaries, fallopian tubes and uterus.

Animal Survival assessment

Cohorts of mice were euthanized by CO_2 asphyxiation at predefined time points to determine disease distribution. Separate cohorts were monitored for survival and euthanized when mice developed a visually distended abdomen resulting from ascites accumulation. Survival was assessed from the date of initial orthotopic tumor inoculation to the date of euthanasia.

Immunohistochemistry and HALO analysis

All studies using human specimens were approved by the Fred Hutchinson Cancer Research Center Institutional Review Board and conducted according to the principles expressed in the Declaration of Helsinki. Tumor tissues were obtained by the POCRC Repository from patients who provided written informed consent. Primary and metastatic mouse tumors were collected at the time of necropsy. Five-micron tissue sections were cut from formalin fixed paraffin-embedded specimens. Hematoxylin and eosin (H&E) and immunohistochemical (IHC) staining for CD31, CD3, CD8, FoxP3, CD45R/B200, and CD68 were performed to characterize the immune composition of the tumor microenvironment as previously described [8]. Slides were then scanned and analyzed using HALO analysis software (Indica Labs).

Gene Expression

RNA was extracted from fresh-frozen primary or metastatic $ID8_{VEGF\text{-}eLuc}$ tumors using the Qiagen RNeasy Plus Mini RNA isolation kit. RNA samples were processed with the Clariom D Pico mouse Assay. Arrays were analyzed using the SST-RMA algorithm in the Affymetrix Transcriptome Analysis Console (TAC) Software. All samples passed quality control criteria established by Affymetrix. Expression data was then imported into R. Probes with less than two arrays above the 95th percentile of the antigenomic background probes were filtered out, leaving 12,884 expressed genes in mouse tumors.

Statistics

For differential gene expression analysis, we used linear models for microarray data (limma Bioconductor package) [16]. A linear model was fitted to each gene, and empirical Bayes moderated t-statistics (2-tailed) were used to assess expression differences. A contrast comparing tumor types (primary mouse tumors v. metastatic mouse tumors) was tested. Intraclass correlations were estimated to account for measures from the same mice. The camera R function was used to perform gene set enrichment analysis (GSEA) for gene sets belonging to the Kyoto Encyclopedia of Genes and Genomes (KEGG) database. These gene sets were downloaded from the MSigDB database version 6.1. A false discovery rate (FDR) cutoff of 5% was used to determine differentially expressed genes and gene sets. Single sample GSEA, an extension of GSEA that calculates separate enrichment scores for each pairing of a sample and gene set, was used for the visualization of gene set scores [17].

Data and software availability

The microarray data have been deposited in NCBI GENE Expression Omnibus (accession number GSE149320).

Results

$ID8_{VEGF\text{-}eLuc}$ cells have enhanced luminescence compared to $ID8_{VEGF\text{-}Luc}$ cells

When 5×10^6 $ID8_{VEGF\text{-}luc}$ cells were injected intraperitoneally, tumor growth was not reliably detectable by *in vivo* imaging (IVIS spectrum) until tumors reached an advanced stage, approximately 10 weeks after injection (Figure 1A). To engineer a version of this cell line that could be detected as micro-metastatic disease, we transduced $ID8_{VEGF}$ cells with an enhanced luciferase construct (eLuc) [13]. *In vitro* IVIS imaging confirmed a significant increase in bioluminescence of $ID8_{VEGF\text{-}eLuc}$ cells compared to $ID8_{VEGF\text{-}Luc}$ cells expressing standard luciferase (Figure 1B). Both smaller numbers of tumor cells and higher luminescence signals/cell were detectable with the enhanced luciferase.

Orthotopic injection of $ID8_{VEGF\text{-}eLuc}$ cells results in disseminated metastatic disease

To model tumor dissemination from a tumor originating in the ovary, we performed orthotopic injection of the $ID8_{VEGF\text{-}eLuc}$ cell line, establishing primary disease under the bursa of the right mouse ovary, and then monitored mice for metastatic progression. As the enhanced luciferase construct can be used to detect as few as 10 cells by IVIS imaging [13], so IVIS bioluminescent imaging was performed 14–18 days after surgery

to confirm the bursa was intact and injected cells had not leaked from the injection site (Figure 1C). Weekly IVIS monitoring revealed a steady bioluminescence increase following tumor inoculation (Figure 1D). Primary ovarian tumors were visualized upon dorsal and ventral imaging. Primary disease was detectable 3 weeks after injection (Figure 1D and 1E) followed by micro-metastatic intraperitoneal disease that became readily visible by 8 weeks. To evaluate metastatic dissemination after orthotopic injection of $ID8_{VEGF\text{-}luc}$ cells, ten mice were inoculated orthotopically with 10^6 tumor cells, two mice from the group sacrificed at every two-week time point, and organs removed for necropsy and immediate IVIS imaging. As early as 2 weeks after tumor inoculation, bioluminescent signals were detectable at necropsy in the right ovary (original injection site). By 4 weeks after tumor inoculation, and at subsequent time points, micro-metastatic disease was detected on peritoneal surfaces, bowel serosa and mesentery, diaphragm, spleen and stomach (Figure 1F), sites commonly involved by metastatic ovarian cancer. This suggested that despite orthotopic ovary-confined tumor inoculation, tumor cells could establish metastatic tumors in locations that recapitulate what is observed in patients.

$ID8_{VEGF\text{-}eLuc}$ cells metastasizing from the ovary progress to terminal hemorrhagic ascites

We next sought to determine the natural progression of disease in this model. Nine mice were orthotopically injected with $ID8_{VEGF\text{-}eLuc}$ cells, IVIS-monitored every 14 days for evidence of metastatic spread, allowed to progress until disease status met euthanasia criteria, and analyzed during necropsy for metastatic disease spread (Figure 2A). All the mice ultimately developed terminal hemorrhagic ascites (Figure 2B), a criterion for euthanasia, and had an enlarged necrotic right ovary (Figure 2C). Necropsy revealed that metastatic tumor developed in numerous sites, including the peritoneum (Figure 2D), diaphragm (Figure 2E), liver and peritoneal bowel surface (Figure 2F), spleen (Figure 2G), and the contralateral ovary (Figure 2H). H&E staining of grossly involved organs confirmed the presence of tumor in the primary site (Figure 2I) and distribution of metastatic disease to the bowel tissue (Figure 2J), pancreas (Figure 2K), liver (Figure 2L), spleen (Figure 2M), peritoneum (Figure 2N), diaphragm (Figure 2O), and lung (Figure 2P).

Cytoreductive surgery can be performed to prolong survival

We then evaluated the impact of cytoreductive surgery on survival in this orthotopic mouse model of ovarian cancer. Two cohorts of mice were inoculated orthotopically with $ID8_{VEGF\text{-}eLuc}$ cells and tumors were allowed to develop for either 6- or 10-weeks, at which point the bilateral ovaries, fallopian tubes, and uterine horns were removed (see Methods, Figure 3A-D). These two time points were chosen to simulate clinical scenarios in which patients may have cytoreductive surgery: either early when micro-metastatic disease may be present, or late when metastatic disease is more likely to be present. At both 6- and 10-week surgical time points, the right ovary was mildly enlarged and no other macroscopic disease was detectable (Figure 3D), and primary tumors were similar in size (Figure 3E), but all mice had bioluminescent evidence of micro-metastatic disease in at least one location. In all cases blood loss was minimal and the mice tolerated surgery well. All mice experienced an initial small weight drop postoperatively but returned to normal weight by postoperative day 10.

Monitoring showed that all mice receiving surgical intervention ultimately developed metastatic disease and terminal hemorrhagic ascites, confirming that metastatic tumors had become established in all mice prior to surgery (Figure 4A). In all experiments, mice consistently developed a distended abdomen that impaired mobility and was the main determinant of survival. Median survival was significantly different between surgical cohorts (Log-rank Mantel-Cox test). The median survival without any cytoreductive surgery was 205 days, while mice that received cytoreduction at 6-weeks (early) survived significantly longer, with a median survival of 360 days (p=0.0107). Mice that underwent cytoreduction at 10-weeks (late), when disease was more advanced, had an intermediate median survival of 241 days, which was not statistically improved over control mice (p=0.1443). Thus, cytoreductive surgery to remove the primary mass could prolong survival, but failed to cure mice, consistent with the evidence of detectable micro-metastases by 6 weeks in our *ex vivo* bioluminescence study.

To determine if cytoreductive surgery impacted immune infiltration into metastatic lesions, IHC was performed on peritoneal metastatic tumors collected at terminal euthanasia from mice that received cytoreductive surgery 6-weeks after tumor injection or mice that did not undergo cytoreductive surgery. IHC staining for CD8 (Figure 4B) and FoxP3 (Figure 4C) showed reduced immune infiltrate in tumors from mice that underwent cytoreductive surgery.

Primary and metastatic tumors have similar immune infiltration

To determine if the immune infiltrate of the mouse tumors recapitulated human disease, we next compared vasculature and immune infiltrates in primary and metastatic tumors from mice and patient samples. IHC staining was performed on primary tumors and metastatic tumors from peritoneal surfaces from mice that underwent orthotopic tumor injection but no cytoreductive surgery, and all samples were obtained when mice reached a terminal endpoint necessitating euthanasia. Primary human tumors were isolated from the ovary and metastatic tumor samples were isolated from peritoneal surfaces or the omentum. Metastatic samples were analyzed separately to control for potential differences. Of note, both primary and metastatic mouse samples were collected at the time of euthanasia, rather than during cytoreduction and at necropsy, because the patient samples we analyzed were collected during the same surgery. IHC staining of formalin-fixed tissue for CD31 (Figure 5A), CD3 (Figure 5B), CD8 (Figure 5C), FoxP3 (Figure 5D), B220/CD20 (Figure 5E), CD68 (Figure 5F) was performed, and the percent positivity in both primary and metastatic tumor quantified using HALO Image Analysis (Figure 5G-L). Vasculature (CD31) was present at similar levels in both murine and human tumors. The infiltrating immune cells included CD8 T cells and CD4 T cells (%$CD3^+$ cells minus %$CD8^+$ T cells), regulatory T cells (Foxp3), B cells (B220/CD20) and tumor-associated macrophages (CD68), and there were no significant differences in the frequency of each of these cell types between primary and metastatic tumors of each species. No significant differences were detected between human metastatic tumors isolated from peritoneal and omental surfaces. No significant differences were detected between murine and human samples for CD31, CD3, CD8, FoxP3, or CD45R/B220 staining (Figure 5G-K, one-way ANOVA for multiple comparisons); however, patient tumors contained significantly more $CD68^+$ cells than murine tumors (Figure 5L).

We previously demonstrated that $ID8_{VEGF}$ tumors developing from intraperitoneal tumor injection and metastatic human high-grade serous ovarian tumors share similar expression of the majority of pathways defined by the KEGG database [8]. However, intraperitoneal tumor injections can only produce metastatic tumors in mice, precluding studies evaluating differences that may arise during seeding of metastatic disease from a primary tumor. To probe potential differences between progressing mouse primary and metastatic tumors in more detail, gene expression by $ID8_{VEGF\text{-}eLuc}$ primary and metastatic peritoneal tumors were compared following deep transcriptome profiling on fresh-frozen samples from mice with tumors injected orthotopically but that did not undergo cytoreductive surgery. To assure comparability between analyzed specimens, all metastatic tumors used for RNA sequencing were isolated from peritoneal surfaces, not omentum. With a 5% false discovery rate (FDR) cutoff, no differentially-expressed genes were found in primary versus metastatic samples, suggesting that dissemination from the primary tumor in this setting does not alter the genetic profile of the ID8 metastatic tumors or represent selection of a distinct subpopulation. To increase the power of the analysis, we then defined gene sets with the KEGG database and evaluated pathways using GSEA. 160 out of 176 KEGG pathways were not statistically different between primary and metastatic tumors (Figure 6). 15 out of 16 differentially-expressed KEGG pathways were related to cellular metabolism (8), insulin (1), Ppar (1), gap junction (1) or Wnt signaling (1), or to pathways associated with the growth of other tumors types (thyroid cancer, basal cell carcinoma, and melanogenesis), and had reduced expression in metastatic tumors (Supplemental Table 1). One KEGG pathway (ribosome) showed increased expression in metastatic tumor samples. Together, these data suggest that the microenvironment differences between tumor growing in the ovarian bursa and tumor growing in the peritoneal cavity can have a small influence on gene expression within $ID8_{VEGF\text{-}eLuc}$ tumors, but do not significantly modulate immune cell infiltration (Figure 5).

Discussion

We have demonstrated that orthotopic injection of $ID8_{VEGF\text{-}eLuc}$ cells into the ovarian bursa of immunocompetent mice is well-tolerated and leads to the development of a progressive primary tumor and widely metastatic ovarian cancer with a disease distribution similar to advanced disease in humans. Previous work showed that orthotopic injection of syngeneic ovarian cancer cells into mouse ovaries is feasible and produces large hyper-vascular primary tumors within 90 days of injection [14]. Development of tumors *in vivo* has been shown to be trackable using IVIS technology, with enhanced luciferase constructs making it feasible to detect very small numbers of cells *in vivo* [13,18]. Our study demonstrates that these technologies can be adapted for monitoring progression of murine ovarian cancer. Although a xenograft model has been used to examine surgical cytoreduction of ovarian cancer, these prior studies required tumors to be grown in immunodeficient mice [19,20], which precludes analysis of the TME or immunosuppressive features of ovarian cancer, thereby limiting what can be assessed with additional interventions. Therefore, we have now combined technologies and strategies to develop a model of micro-metastatic disease that can be used to evaluate surgical cytoreduction and potentially subsequent therapeutic interventions, in an immunocompetent mouse model of ovarian cancer.

Current transplantable murine models of ovarian cancer that use intraperitoneal injection do generate tumors that recapitulate many immunosuppressive features of human disease [8], but many treatments in these models are performed shortly after tumor cells are injected. The biology of ovarian tumor metastases is not completely understood, and studies initiated shortly after intraperitoneal tumor cell injection may reflect effects on the requirements for tumor cell engraftment rather than on treatment of micro-metastatic tumor in its established niche or minimal residual disease. We sought to develop a preclinical model in which the tumor is established and has developed its associated TME, and in which treatment options for physiologically relevant minimal residual disease could be assessed following surgical cytoreduction, which closely approximates the common clinical treatment paradigm in human ovarian cancer. As all mice that receive cytoreductive surgery develop and succumb to progressive metastatic disease, this model establishes a treatment window for assessing novel therapeutics targeting micro-metastatic disease.

Notably, when we characterized the TME in this model, no significant differences were found between primary and metastatic mouse tumors in immune composition or gene expression, similar to what has been reported in human colorectal cancer and renal cell carcinoma [21]. The extensive similarities between primary and metastatic tumors confirms that the disseminating cells that establish metastatic tumors in our model do not undergo significant genetic changes essential for making metastasis feasible or result from the outgrowth of rare subclones with a unique profile. This consistency between primary and metastatic tumor microenvironments and the limited mouse-to-mouse variation in tumor development is particularly useful in the context of demonstrating the model's reproducibility. Of note, our findings in the mouse model do contrast with an individual case study performed on tissue from an ovarian cancer patient with multiple sites of metastatic disease [22], but this may reflect mutagenesis and/or selection from prior chemotherapy exposure (the patient had received multiple rounds of chemotherapy with nine distinct agents). However, it may alternatively imply that the model described here may have greater utility in modeling frontline treatment strategies, including targeted therapies.

This study serves as a proof-of-concept that orthotopic injection of transplantable ovarian tumor cells, combined with surgical cytoreduction, can be used to establish minimal residual disease or late-stage metastatic tumors. Our studies were performed using the $ID8_{VEGF}$ model, and previous analysis of the TME has shown that it recapitulates most of the suppressive features of the ovarian TME [8]. We previously reported that immune infiltration and gene expression of pathways that influence the immune response were strikingly similar between the mouse model and human disease, with the exception of differences in expression of several metabolic pathways [8]. Here, using IHC analysis, we noted mostly similar immune infiltration between species, with one important difference: both the primary and metastatic mouse tumors had significantly less myeloid cell infiltration than human tumors. This suggests that the $ID8_{VEGF\text{-}eLuc}$ model may not be broadly predictive for studies evaluating targeting of myeloid cell components or metabolic pathways.

In part, the disparities observed between this model and patient samples may reflect that human ovarian cancer has multiple distinct subtypes [23], and high-grade serous

ovarian cancer has been further subdivided by molecular and histologic phenotype into mesenchymal, immunoreactive, differentiated, and proliferative subgroups [23–25]. Given the lack of desmoplasia, low immune cell infiltration, and minimal papillary/glandular architecture, $ID8_{VEGF}$ tumors exhibit histologic characteristics consistent with the proliferative subtype. One limitation of the $ID8_{VEGF}$ cell line is that it does not contain a p53 mutation, which is commonly detected in ovarian cancers. Recently developed transplantable models, such as those employing CRISPR-edited ID8 tumors [7] or mouse high-grade serous ovarian cancer cell lines derived from a genetically-engineered mouse model containing p53, PTEN and/or BRCA mutations ("HGS1–4") [26], have been shown to individually recapitulate some of the different histologic pathologies observed in patients. For example, HGS1–4 tumor cell lines recapitulate the stromal composition and vascular architecture of human ovarian cancer, but tumors derived from four different HGS cell lines exhibited different immune cell infiltration profiles [26], as with human ovarian cancers. Thus, transduction of different ovarian cancer cell lines with enhanced luciferase could be used with the surgical cytoreduction approach described here to develop models for evaluating the efficacy of new therapies in micro-metastatic minimal residual disease settings that reflect the other disease subtypes observed in patients.

While we have successfully constructed a murine model that incorporated both local tumorigenesis within the ovary/fallopian tube microenvironment and therapeutically beneficial surgical cytoreduction, we did encounter a potential limitation for evaluation of post-surgical therapeutic strategies. Notably, surgical cytoreduction significantly delayed the development of clinically evident disease, pushing survival to 12 months post cytoreduction, which may adequately mimic human disease but makes survival a protracted and thus difficult research end-point. However, to overcome this issue of extended survival, IVIS-measured tumor growth or disappearance may be used as a more immediate alternative method to evaluate treatment efficacy. Notably, our study suggests that while both the intraperitoneal and surgical models appear adequate for interrogating advanced stage disease, the intraperitoneal model may be more appropriate for such studies because it is faster and easier to use. However, to address questions related to therapy of micro-metastatic disease, the surgical model results in minimal residual disease seeding from the primary tumor and is more likely to reflect the biology of newly spontaneously established metastatic tumor cells that will otherwise progress to advanced stage disease.

There is increasing focus on the role for immunotherapy in the treatment of patients with gynecologic cancers. Although response rates in ovarian cancer remain currently low [27,28], ovarian cancer is perceived as a potentially immunogenic tumor, with significantly improved survival rates are observed in the subset of patients that exhibit lymphocyte infiltration [29–31]. Notably, the presence of suppressive $FoxP3^+$ regulatory T cells in ovarian cancer correlates with reduced patient survival [32], further supporting the relevance of the host anti-tumor immune response in ovarian cancer. Therefore, newer immunotherapy strategies are being actively pursued, and it may be essential to evaluate and deploy these approaches in patients with small volume disease, in which such therapy may be more efficacious [33–35]. Notably, we observed a reduction in immune infiltration in metastatic tumors that developed after surgical cytoreduction that may have implications for the efficacy of some treatment regimens. For example, immunotherapies that enhance the

anti-tumor function of tumor-infiltrating T cells may be less effective if fewer T cells are present at the time of treatment. This observation may also influence the use of combination therapies that improve T cell recruitment to tumors. Further studies in this model could yield insights about the timing of surgery and subsequent treatments. Pre-clinical models that facilitate evaluation of the efficacy of new small molecules, chemotherapeutic agents, or immunotherapy in minimal residual disease may yield critical insights, and foster advancing their translation into the care of patients with ovarian cancer.

Supplementary Material

Refer to Web version on PubMed Central for supplementary material.

Acknowledgements:

The authors thank Dr. Matthias Stephan for sharing the ID8$_{VEGF}$ and ID8$_{VEGF\text{-}luc}$ cell lines, Dr. Patrick Hwu for generously gifting the enhanced luciferase construct for these studies, members of the FHCRC histology core (Savanh Chanthaphavong, Tracy Goodpaster, Li-Ya Huang, Nasreen Bhatti, Paul Kong) and the UW histology core (Brian Johnson and Megan Larmore) for histopathology assistance, members of FHCRC Comparative Medicine (Jennifer Duncan, Jamie Nguyen, Merry Wick, and Lisa Paul) for animal and IVIS imaging assistance, Dr. Deborah Banker for manuscript revision, and members of the Greenberg lab for discussion and constructive feedback.

Funding: This work was supported by NIH T32CA009515 (to C.B.M.), a Colleen's Dream Foundation award (to K.G.A.), the OCRA Ann and Sol Schreiber Mentored Investigator Award (to K.G.A), and a research agreement with Juno Therapeutics (to P.D.G). The content is solely the responsibility of the authors and does not necessarily represent the official views of the NIH.

Conflict of Interest statement: P.D.G. has patents with, received funding from, and was a scientific consultant to Juno Therapeutics. R.G. has received consulting income from Juno Therapeutics, Takeda, Infotech Soft, Celgene, Merck and has received research support from Janssen Pharmaceuticals and Juno Therapeutics, and declares ownership in CellSpace Biosciences.

References

[1]. Siegel RL, Miller KD, Jemal A, Cancer statistics, 2019., CA. Cancer J. Clin 69 (2019) 7–34. doi:10.3322/caac.21551. [PubMed: 30620402]

[2]. Vaughan S. et al. , Rethinking ovarian cancer: recommendations for improving outcomes., Nat. Rev. Cancer 11 (2011) 719–25. doi:10.1038/nrc3144. [PubMed: 21941283]

[3]. Santoiemma PP, Powell DJ, Tumor infiltrating lymphocytes in ovarian cancer., Cancer Biol. Ther 16 (2015) 807–20. doi:10.1080/15384047.2015.1040960. [PubMed: 25894333]

[4]. Zsiros E, Tanyi J, Balint K, Kandalaft LE, Immunotherapy for ovarian cancer: recent advances and perspectives., Curr. Opin. Oncol 26 (2014) 492–500. doi:10.1097/CCO.0000000000000111. [PubMed: 25036883]

[5]. Roby KF et al. , Development of a syngeneic mouse model for events related to ovarian cancer., Carcinogenesis. 21 (2000) 585–91. doi:10.1093/carcin/21.4.585. [PubMed: 10753190]

[6]. Zhang L. et al. , Generation of a syngeneic mouse model to study the effects of vascular endothelial growth factor in ovarian carcinoma., Am. J. Pathol 161 (2002) 2295–309. doi:10.1016/s0002-9440(10)64505-1. [PubMed: 12466143]

[7]. Walton JB et al. , CRISPR/Cas9-derived models of ovarian high grade serous carcinoma targeting Brca1, Pten and Nf1, and correlation with platinum sensitivity., Sci. Rep 7 (2017) 16827. doi:10.1038/s41598-017-17119-1. [PubMed: 29203787]

[8]. Anderson KG et al. , Engineered Adoptive T-cell Therapy Prolongs Survival in a Preclinical Model of Advanced-Stage Ovarian Cancer., Cancer Immunol. Res 7 (2019) 1412–1425. doi:10.1158/2326-6066.CIR-19-0258. [PubMed: 31337659]

[9]. Guo Z, Wang H, Meng F, Li J, Zhang S, Combined Trabectedin and anti-PD1 antibody produces a synergistic antitumor effect in a murine model of ovarian cancer., J. Transl. Med 13 (2015) 247. doi:10.1186/s12967-015-0613-y. [PubMed: 26219551]

[10]. Zhu X, Xu J, Cai H, Lang J, Carboplatin and programmed death-ligand 1 blockade synergistically produce a similar antitumor effect to carboplatin alone in murine ID8 ovarian cancer model., J. Obstet. Gynaecol. Res 44 (2018) 303–311. doi:10.1111/jog.13521. [PubMed: 29171115]

[11]. Chang SJ, Bristow RE, Chi DS, Cliby WA, Role of aggressive surgical cytoreduction in advanced ovarian cancer., J. Gynecol. Oncol 26 (2015) 336–42. doi:10.3802/jgo.2015.26.4.336. [PubMed: 26197773]

[12]. Dao F. et al. , Characteristics of 10-year survivors of high-grade serous ovarian carcinoma., Gynecol. Oncol 141 (2016) 260–263. doi:10.1016/j.ygyno.2016.03.010. [PubMed: 26968641]

[13]. Rabinovich BA et al. , Visualizing fewer than 10 mouse T cells with an enhanced firefly luciferase in immunocompetent mouse models of cancer., Proc. Natl. Acad. Sci. U. S. A 105 (2008) 14342–6. doi:10.1073/pnas.0804105105. [PubMed: 18794521]

[14]. Greenaway J, Moorehead R, Shaw P, Petrik J, Epithelial-stromal interaction increases cell proliferation, survival and tumorigenicity in a mouse model of human epithelial ovarian cancer., Gynecol. Oncol 108 (2008) 385–94. doi:10.1016/j.ygyno.2007.10.035. [PubMed: 18036641]

[15]. Greenaway JB et al. , Ovarian tumour growth is characterized by mevalonate pathway gene signature in an orthotopic, syngeneic model of epithelial ovarian cancer., Oncotarget. 7 (2016). doi:10.18632/oncotarget.10121.

[16]. Ritchie ME et al. , limma powers differential expression analyses for RNA-sequencing and microarray studies., Nucleic Acids Res. 43 (2015) e47. doi:10.1093/nar/gkv007. [PubMed: 25605792]

[17]. Rahmatallah Y, Emmert-Streib F, Glazko G, Gene set analysis approaches for RNA-seq data: performance evaluation and application guideline., Brief. Bioinform 17 (2016) 393–407. doi:10.1093/bib/bbv069. [PubMed: 26342128]

[18]. Nunez-Cruz S, Connolly DC, Scholler N, An orthotopic model of serous ovarian cancer in immunocompetent mice for in vivo tumor imaging and monitoring of tumor immune responses., J. Vis. Exp (2010) 2–5. doi:10.3791/2146.

[19]. Helland Ø et al. , First in-mouse development and application of a surgically relevant xenograft model of ovarian carcinoma, PLoS One. 9 (2014). doi:10.1371/journal.pone.0089527.

[20]. Helland Ø et al. , The HDACi Panobinostat Shows Growth Inhibition Both In Vitro and in a Bioluminescent Orthotopic Surgical Xenograft Model of Ovarian Cancer., PLoS One. 11 (2016) e0158208. doi:10.1371/journal.pone.0158208. [PubMed: 27352023]

[21]. Remark R. et al. , Characteristics and clinical impacts of the immune environments in colorectal and renal cell carcinoma lung metastases: influence of tumor origin., Clin. Cancer Res 19 (2013) 4079–91. doi:10.1158/1078-0432.CCR-12-3847. [PubMed: 23785047]

[22]. Jiménez-Sánchez A. et al. , Heterogeneous Tumor-Immune Microenvironments among Differentially Growing Metastases in an Ovarian Cancer Patient, Cell. 170 (2017) 927–938.e20. doi:10.1016/j.cell.2017.07.025. [PubMed: 28841418]

[23]. Cancer Genome Atlas Research Network et al. , Integrated genomic analyses of ovarian carcinoma, Nature. 474 (2011) 609–615. doi:10.1038/nature10166. [PubMed: 21720365]

[24]. Verhaak RGW et al. , Prognostically relevant gene signatures of high-grade serous ovarian carcinoma., J. Clin. Invest 123 (2013) 517–25. doi:10.1172/JCI65833. [PubMed: 23257362]

[25]. Murakami R. et al. , Establishment of a Novel Histopathological Classification of High-Grade Serous Ovarian Carcinoma Correlated with Prognostically Distinct Gene Expression Subtypes., Am. J. Pathol 186 (2016) 1103–13. doi:10.1016/j.ajpath.2015.12.029. [PubMed: 26993207]

[26]. Maniati E. et al. , Mouse Ovarian Cancer Models Recapitulate the Human Tumor Microenvironment and Patient Response to Treatment., Cell Rep. 30 (2020) 525–540.e7. doi:10.1016/j.celrep.2019.12.034. [PubMed: 31940494]

[27]. Hamanishi J. et al. , Safety and antitumor activity of Anti-PD-1 antibody, nivolumab, in patients with platinum-resistant ovarian cancer, J. Clin. Oncol 33 (2015) 4015–4022. doi:10.1200/JCO.2015.62.3397. [PubMed: 26351349]

[28]. Disis ML et al. , Efficacy and Safety of Avelumab for Patients With Recurrent or Refractory Ovarian Cancer: Phase 1b Results From the JAVELIN Solid Tumor Trial., JAMA Oncol. 5 (2019) 393–401. doi:10.1001/jamaoncol.2018.6258. [PubMed: 30676622]

[29]. Zhang L. et al. , Intratumoral T cells, recurrence, and survival in epithelial ovarian cancer., N. Engl. J. Med 348 (2003) 203–13. doi:10.1056/NEJMoa020177. [PubMed: 12529460]

[30]. Hinchcliff E. et al. , Lymphocyte-specific kinase expression is a prognostic indicator in ovarian cancer and correlates with a prominent B cell transcriptional signature., Cancer Immunol. Immunother 68 (2019) 1515–1526. doi:10.1007/s00262-019-02385-x. [PubMed: 31515669]

[31]. Kroeger DR, Milne K, Nelson BH, Tumor-Infiltrating Plasma Cells Are Associated with Tertiary Lymphoid Structures, Cytolytic T-Cell Responses, and Superior Prognosis in Ovarian Cancer., Clin. Cancer Res 22 (2016) 3005–15. doi:10.1158/1078-0432.CCR-15-2762. [PubMed: 26763251]

[32]. Curiel TJ et al. , Specific recruitment of regulatory T cells in ovarian carcinoma fosters immune privilege and predicts reduced survival, Nat. Med 10 (2004) 942–949. doi:10.1038/nm1093. [PubMed: 15322536]

[33]. Wen FT, Thisted RA, Rowley DA, Schreiber H, A systematic analysis of experimental immunotherapies on tumors differing in size and duration of growth., Oncoimmunology. 1 (2012) 172–178. doi:10.4161/onci.1.2.18311. [PubMed: 22720238]

[34]. Katsurada M. et al. , Baseline Tumor Size as a Predictive and Prognostic Factor of Immune Checkpoint Inhibitor Therapy for Non-small Cell Lung Cancer., Anticancer Res. 39 (2019) 815–825. doi:10.21873/anticanres.13180. [PubMed: 30711962]

[35]. Tumor Burden Affects Efficacy of Combination Immunotherapy, Cancer Discov. 9 (2019) OF11–OF11. doi:10.1158/2159-8290.CD-RW2019-021.

Highlights:

- Orthotopic tumor inoculation establishes a progressive primary tumor that disseminates to form metastatic disease.
- Metastases recapitulate the immune profile of the originating primary tumor and metastatic human disease.
- Surgical cytoreduction of primary tumors prolongs survival.
- Surgical cytoreduction retains micro-metastatic disease for evaluating therapeutic interventions.

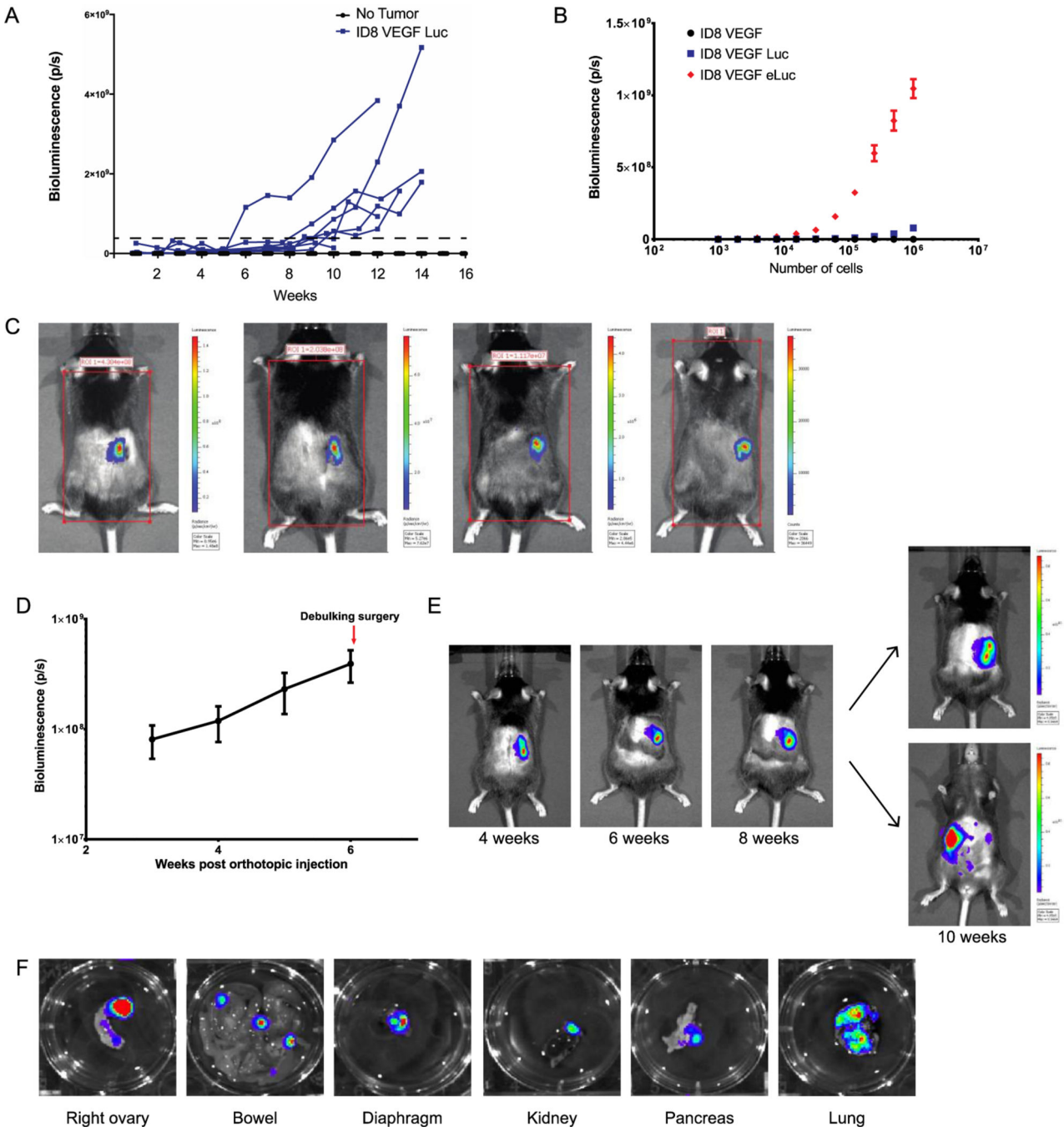

Figure 1. ***In vitro*** **and** ***in vivo*** **bioluminescence of ID8$_{VEGF}$ cells.**

(A) Bioluminescence of ID8$_{VEGF}$ cells transduced with luciferase (Luc) after intraperitoneal (IP) injection. Each line represents one mouse injected with 5×10^6 cells. Dashed line represents defined "detectable" disease. p/s = photons per second. (B) Bioluminescence of ID8VEGF cells transduced with luciferase or an enhanced luciferase (eLuc) construct. Data represent 3 samples per condition. Errors bars represent SD. (C) Representative bioluminescent images from 4 mice 14 days after orthotopic injection. Images from 4 independent experiments. (D) Monitoring bioluminescence *in vivo* following orthotopic

injection into the right ovary. Data averaged from 20 mice. Errors bars represent SD. (E) Evidence of progression at primary site of disease with micro-metastatic disease becoming detectable in this mouse at 10 weeks. Images are from one mouse, as representative of 20 mice. Of note, most mice show signal indicative of micro-metastatic disease development by 6 weeks after tumor injection. (F) Representative images from various organs showing bioluminescence from micro-metastatic disease. Images of organs from 2 mice 4 weeks after tumor injection.

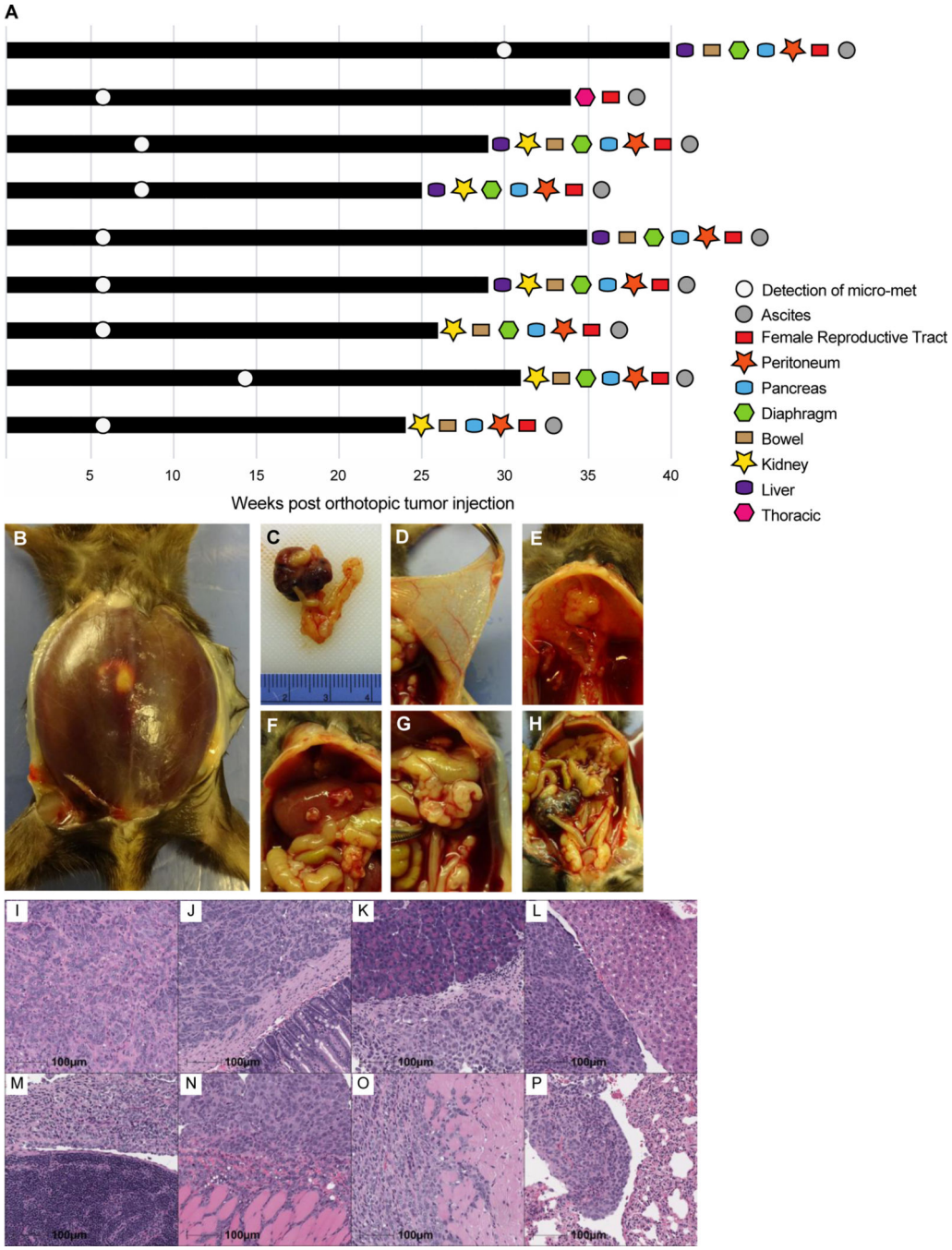

Figure 2. Development of metastatic disease in mice after orthotopic injection of ID8$_{VEGF\text{-}eLuc}$ cells.

(A) Swimmer's plot outlining disease progression and the tissues found to contain gross metastatic disease at necropsy after euthanasia in 9 mice. (B) Hemorrhagic ascites present at time of euthanasia. (C) Large primary tumor after orthotopic injection into right ovarian bursa. (D) Peritoneal-based miliary disease. (E) Diaphragmatic plaques. (F) Liver surface involvement. (G) Splenic involvement. (H) Large primary tumor compared to contralateral ovary. H&E stains of (I) primary tumor, and metastatic tumor to (J) bowel, (K) pancreas, (L)

liver, (M) spleen, (N) peritoneum, (O) diaphragm, and (P) lung. Scale bars represent 100 μm. Images are representative of H&E staining from 20 mice.

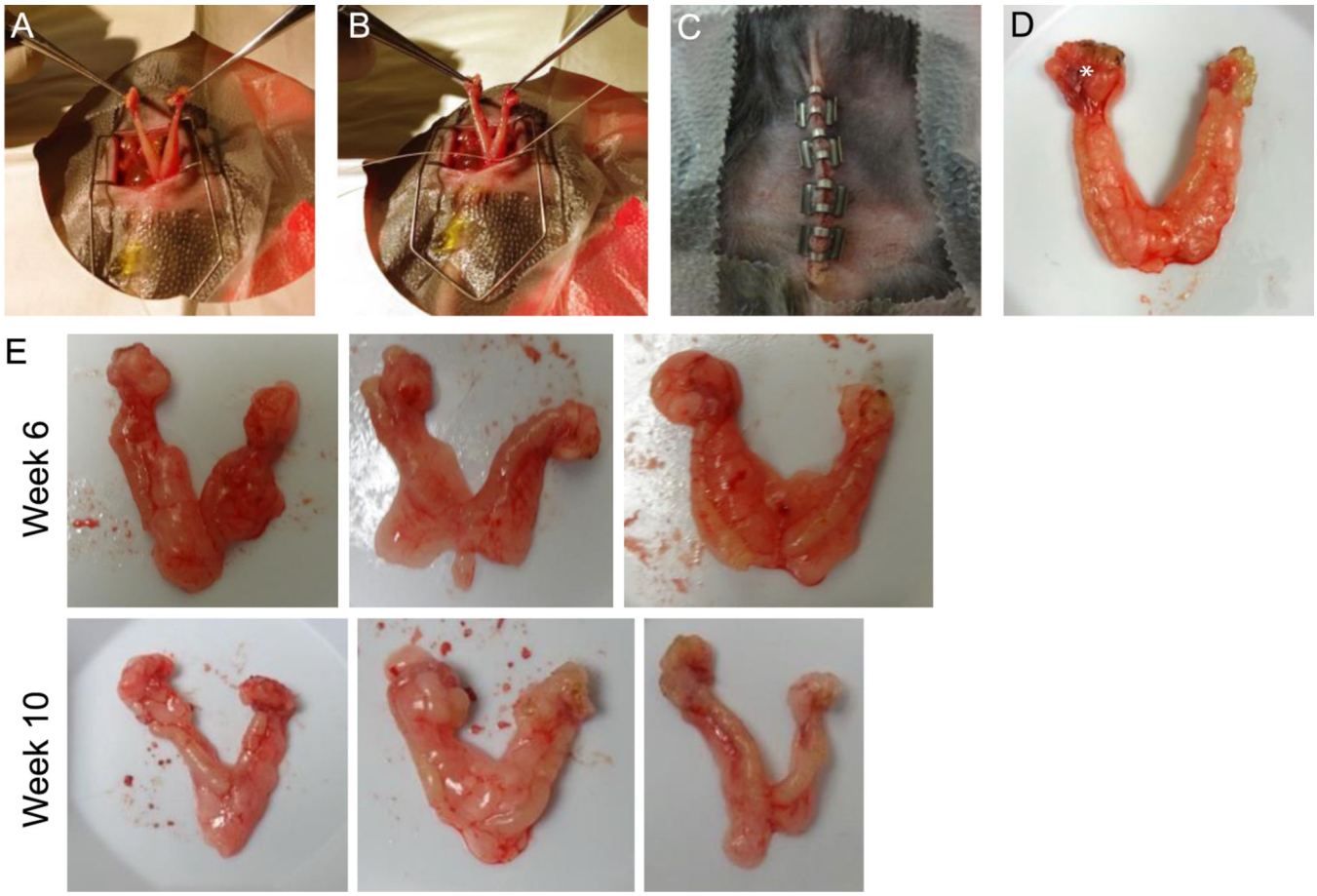

Figure 3. Surgical procedures and surgical specimen after orthotopic injection.

(A) Midline entry into the abdominal cavity with exposure of the bilateral ovaries, fallopian tubes, and uterus. (B) Single suture ligature at the base of the two uterine horns prior to excising the specimen. (C) Closed abdominal cavity with clips inserted at the end of the procedure. (D) Surgical specimen after surgical cytoreduction showing enlarged tumor-bearing right ovary (*). (E) 3 Representative images of surgical specimens from 6- or 10-week cytoreduction. Images are representative of 60 mice from 3 independent experiments.

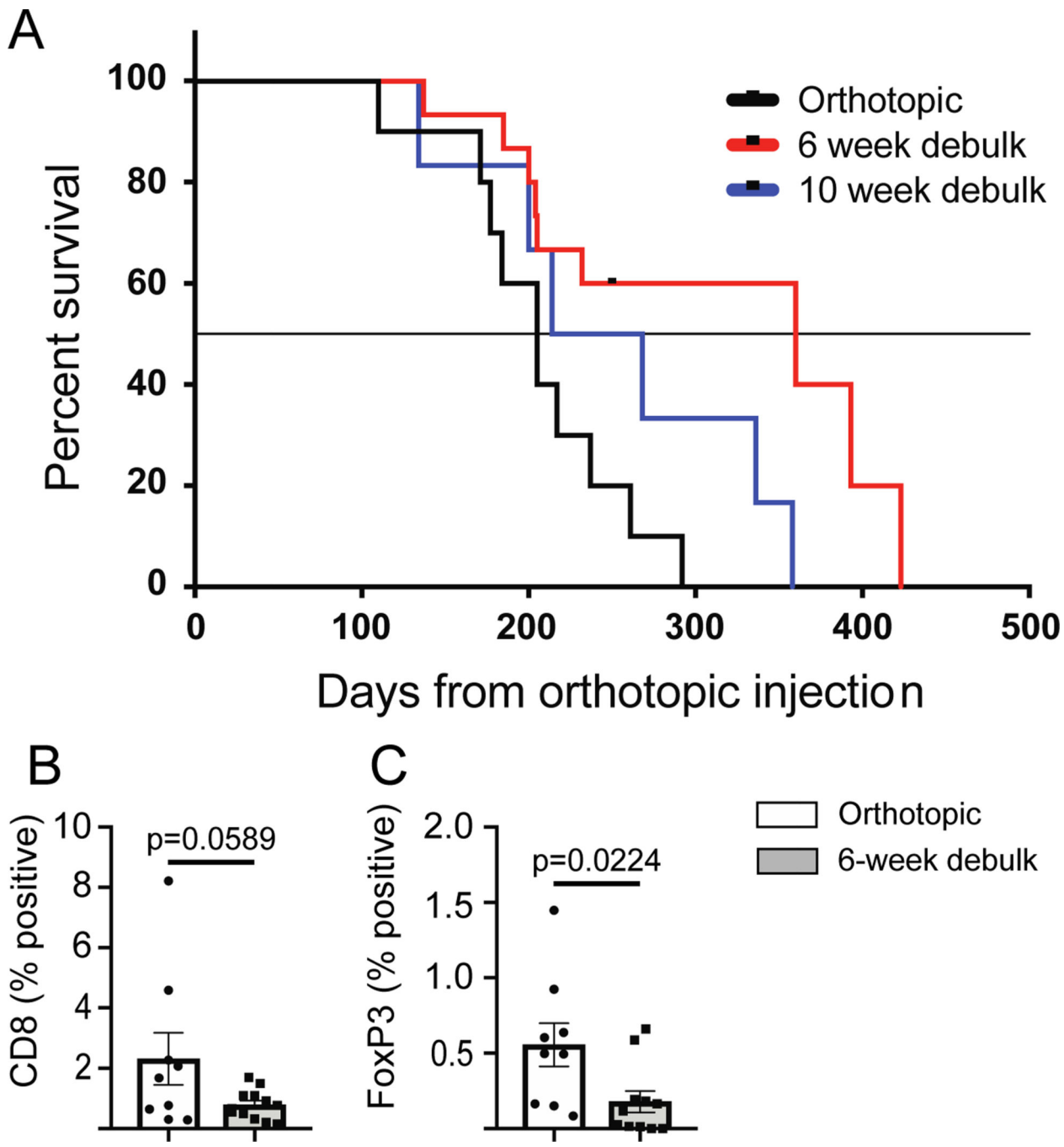

Figure 4. Survival after orthotopic injection with or without cytoreductive surgery.

A) Control mice received no surgical intervention. Treated mice received a hysterectomy and bilateral salpingo-oophorectomy at either 6- or 10-weeks after tumor inoculation. Without cytoreductive surgery mice lived for a median of 205 days (n=10). After late (10 week) cytoreductive surgery, there was an intermediate survival of a median of 241 days (n=6; p=0.1443 compared to no surgery control). After early (6 week) cytoreductive surgery, mice experienced the longest survival, with a median of 360 days (n=15; p=0.0107 compared to no surgery control). Black dash in the 6-week cohort indicates when a group of mice was

censored from the study. Statistical analysis performed using a Log-rank Mantel-Cox test. IHC for B) CD8 or C) FoxP3 was performed on metastatic tumor samples from mice that did not receive cytoreductive surgery (white box, n=9) or that received 6-week cytoreductive surgery (gray box, n=11–12). Statistical analysis performed using an unpaired student's t-test.

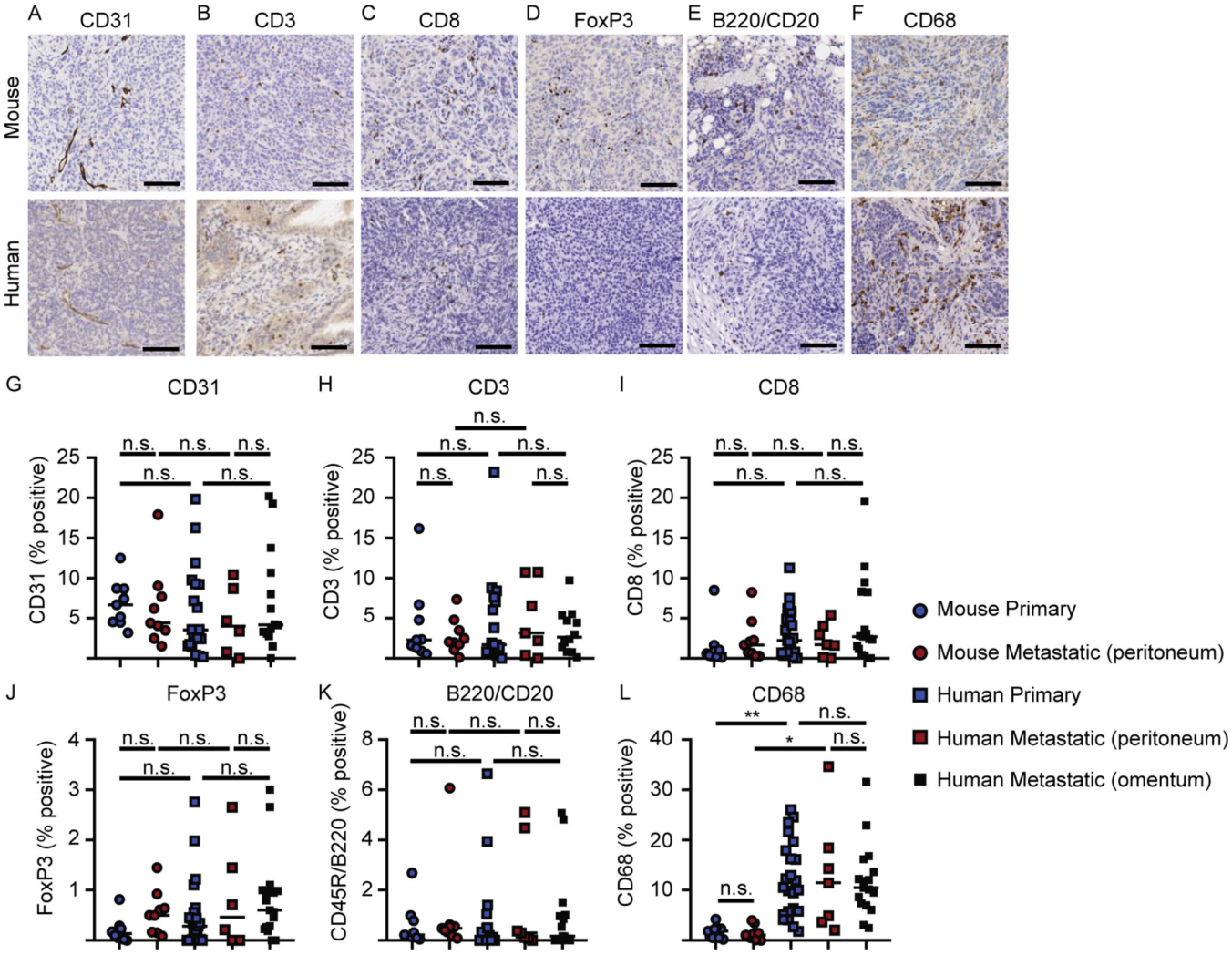

Figure 5. Immunohistochemistry of primary and metastatic tumors.

IHC staining was performed on primary or metastatic tumors from peritoneal surfaces from mice that underwent orthotopic tumor injection but no cytoreductive surgery, and all samples were obtained when mice reached a terminal endpoint necessitating euthanasia. Representative images of (A) CD31, (B) CD3, (C) CD8, (D) FoxP3, (E) B220/CD20, and (F) CD68 from mouse or human samples, respectively. Percent cells positive for the defined molecule from primary and metastatic mouse and human tumors (G) CD31, (H) CD3, (I) CD8, (J) FoxP3, (K) B220/CD20, and (L) CD68, respectively. Scale bars represent 100 μm. Images (A-F) are representative of 9 primary mouse tumors and 19–24 primary human tumors. Data (G-L) from 9 mice per group, 19–24 patient samples per group. Statistical analysis was performed using one way ANOVA for multiple comparisons.

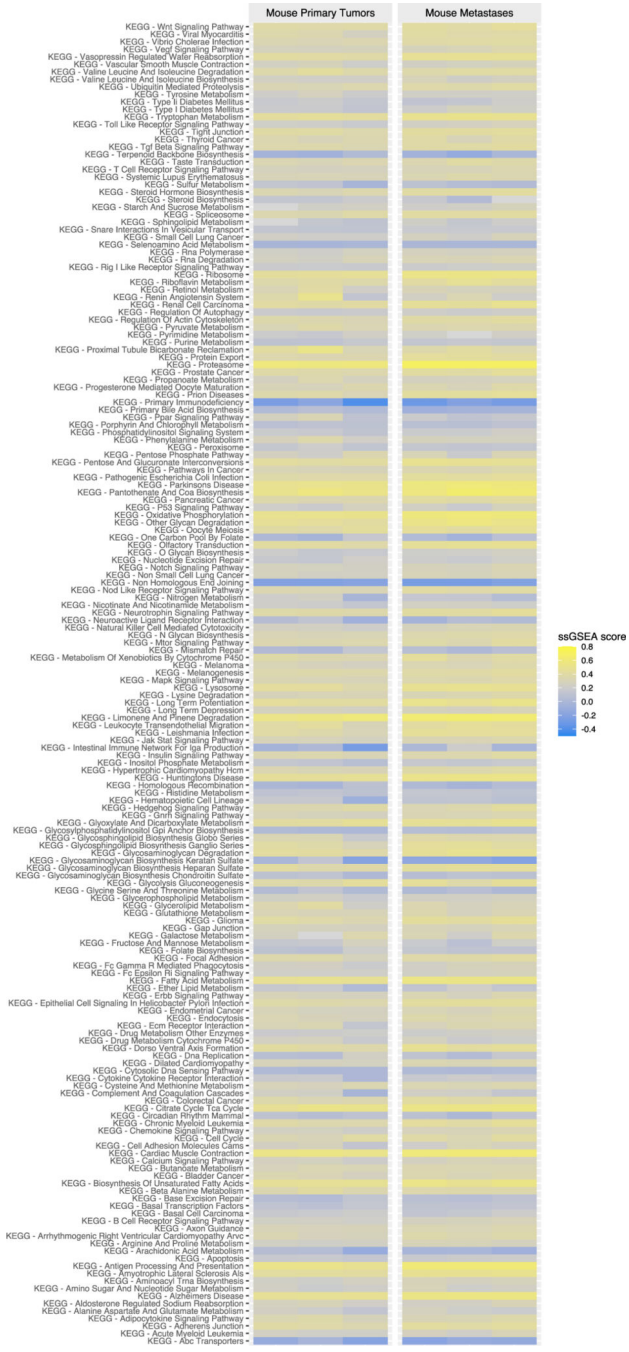

Figure 6. Deep transcriptome profiling of primary and metastatic ID8$_{VEGF\text{-}eLuc}$ ovarian tumors.

RNA expression was evaluated in primary and peritoneal metastatic tumors from mice that underwent orthotopic tumor injection but no cytoreductive surgery, and all samples were obtained when mice reached a terminal endpoint necessitating euthanasia. 160 of 176 KEGG pathways revealed no significant differences (FDR 5%) between primary and metastatic mouse tumor samples. Data obtained from 3 primary mouse tumors and 3 metastatic mouse

tumors isolated from the peritoneum. ssGSEA, an extension of GSEA, was used to visualize gene set enrichment scores for each pairing of a sample and gene set.